

mmWEAVER: Environment-Specific mmWave Signal Synthesis from a Photo and Activity Description

Mahathir Monjur
UNC Chapel Hill
mahathir@cs.unc.edu

Shahriar Nirjon
UNC Chapel Hill
nirjon@cs.unc.edu

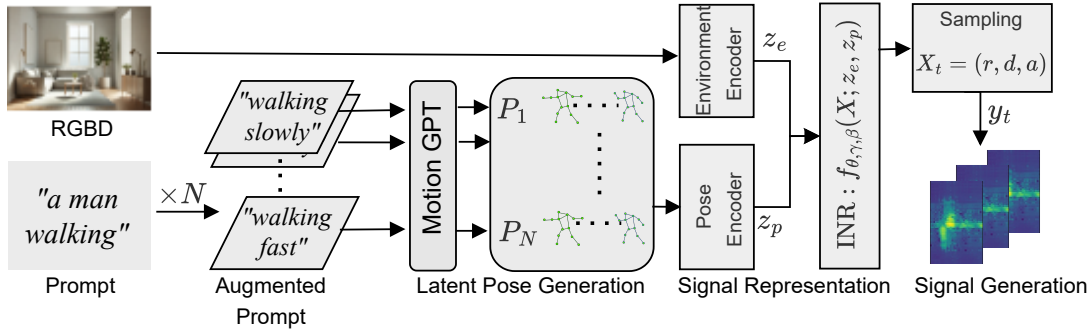


Figure 1. System overview of mmWeaver. Given an RGB-D image and a textual activity description, MotionGPT generates human pose sequence. The environment encoder extracts static scene features (z_e) from RGB, depth, and segmentation maps, while the pose encoder processes the pose sequence to produce temporally-aware motion features ($\{z_p\}_t$). These are fused and input into a hypernetwork that generates the weights (θ) and time-based modulation parameters ($\gamma(t), \beta(t)$) for an Implicit Neural Representation (INR), which models the mmWave signal as a continuous function. The INR is then sampled over spatial-temporal coordinates to synthesize high-resolution mmWave signals tailored to the environment and motion context.

Abstract

Realistic signal generation and dataset augmentation are essential for advancing mmWave radar applications such as activity recognition and pose estimation, which rely heavily on diverse, and environment-specific signal datasets. However, mmWave signals are inherently complex, sparse, and high-dimensional, making physical simulation computationally expensive. This paper presents mmWeaver, a novel framework that synthesizes realistic, environment-specific complex mmWave signals by modeling them as continuous functions using Implicit Neural Representations (INRs), achieving up to 49-fold compression. mmWeaver incorporates hypernetworks that dynamically generate INR parameters based on environmental context (extracted from RGB-D images) and human motion features (derived from text-to-pose generation via MotionGPT), enabling efficient and adaptive signal synthesis. By conditioning on these semantic and geometric priors, mmWeaver generates diverse I/Q signals at multiple resolutions, preserving phase information critical for downstream tasks such as point cloud es-

imation and activity classification. Extensive experiments show that mmWeaver achieves a complex SSIM of 0.88 and a PSNR of 35 dB, outperforming existing methods in signal realism while improving activity recognition accuracy by up to 7% and reducing human pose estimation error by up to 15%, all while operating 6–35× faster than simulation-based approaches.

1. Introduction

mmWave sensing is a promising technology for indoor applications such as patient monitoring [12, 34, 35], activity recognition [19, 28], and pose estimation [1, 14, 16, 18], offering key advantages over traditional vision systems. Unlike optical cameras, mmWave radars preserve privacy by avoiding detailed imaging, making them ideal for sensitive environments like homes and healthcare settings. They function well in low-light conditions and can penetrate clothing and some walls, enabling robust motion tracking. However, factors such as environmental sensitivity, room

layout variation, material properties and deployment cost pose significant challenges to widespread adoption.

Synthetic mmWave data generation has emerged as a promising solution to dataset scarcity, offering a rapid and cost-effective alternative to large-scale data collection. Techniques such as data augmentation through transformations [30], RF simulations [4, 27, 30], and model-based generative methods [5, 8, 32, 36] enhance dataset diversity and improve model robustness. However, generative models often fail to incorporate environment-specific details, overlooking critical propagation effects unique to indoor settings. Simulation-based methods, though reliable in idealized empty environments, are computationally expensive and may not reflect the noise and variability of real-world data.

When the deployment environment is known, we advocate for environment-specific synthetic data generation, which offers greater accuracy than generic augmentation. Effective tools for this task should satisfy three criteria: (i) generate realistic data that capture both human motion and environment-specific characteristics, (ii) require minimal yet informative inputs encoding scene and activity context, and (iii) produce mmWave signals in a storage-efficient, shareable, and resolution-scalable format suitable for diverse applications.

In this paper, we introduce *mmWeaver*, a framework that generates environment-specific mmWave signals for diverse human activities from two simple inputs: a photo of the room (capturing geometry, objects, and materials) and a textual activity description (e.g., “*user seated on couch drinking water*”). *mmWeaver* synthesizes realistic signals that reflect human gestures and movements in the target environment, employs a space-efficient representation to address storage and sharing limits, and supports multi-resolution sampling via parameterized data representations. It also avoids overfitting to minor environmental changes and enables large-scale dataset creation through unlimited input-output variations. By reducing costly real-world data collection, *mmWeaver* facilitates reuse of synthetic data across diverse sensing and AI applications.

Modeling mmWave signal propagation in indoor environments is challenging due to complex interactions between static factors (e.g., multipath from walls and furniture) and dynamic factors (e.g., body shape, pose, and motion). To address this, we propose *mmWeaver*, which leverages Implicit Neural Representations (INRs) [20] to model signals as continuous, differentiable functions, enabling multi-resolution synthesis and compact storage. To adapt across scenarios, *mmWeaver* uses hypernetworks [24] that generate INR weights conditioned on two modalities: an *environment encoder*, extracting spatial priors from room images, and a *pose encoder*, capturing human motion features. A generative model further augments realistic motion

diversity, ensuring *mmWeaver* produces semantically accurate, environment- and activity-specific mmWave signals.

Our INR-hypernetwork architecture generalizes across unseen environments while supporting applications such as data augmentation, signal super-resolution, and compact storage. To our knowledge, *mmWeaver* is the first framework to unify continuous INR-based RF modeling with context-driven hypernetwork adaptation. Compared to prior work (e.g., RF-Genesis with 20–120s inference time), *mmWeaver* synthesizes realistic, environment-specific signals in just 3.4s per activity, enabling efficient, real-time deployment without requiring additional data collection or user-specific retraining.

To demonstrate *mmWeaver*’s efficacy, we conduct extensive experiments using data from 10 indoor scenes and 12 human activities. The dataset includes synchronized mmWave radar signals, RGB-D images, and human pose sequences captured via motion capture systems. Our experiments show *mmWeaver* achieves a complex SSIM of 0.88 and PSNR of 35 dB, outperforming existing methods. Using *mmWeaver*-augmented datasets improves activity recognition accuracy by up to 7% and reduces MPJPE in pose estimation by 15%, demonstrating its effectiveness for mmWave signal generation and augmentation. Additionally, experiments on the publicly available HuPR [14] dataset show that *mmWeaver*-synthesized and augmented data improves pose estimation performance by up to 10%.

2. Related Work

Implicit Neural Representations (INRs) and Hypernetworks: INRs have emerged as a powerful framework for modeling high-dimensional data as continuous functions [20, 22, 23]. By parameterizing signals as neural networks, they enable efficient encoding, interpolation, and super-resolution. While widely applied in computer vision tasks such as image compression [22] and 3D reconstruction [33], their use for spatiotemporal radar signals remains underexplored. Hypernetworks [6], which dynamically generate weights for other networks, have shown strong synergy with INRs in image [21] and audio domains [24, 24], but their potential for radar signal generation is only beginning to be explored.

Applications of mmWave Signals: mmWave signals support tasks such as human pose estimation [1, 14, 16, 18, 31], activity recognition [19, 28], and gesture recognition [15], but their performance often degrades in unseen environments due to RF noise. Few-shot adaptation methods alleviate this but require new data collection, while approaches like *mmClip* [3] target unseen activities rather than environment variation. In contrast, *mmWeaver* generates environment-specific synthetic signals, improving robustness of mmWave systems for both traditional models and few/zero-shot activity recognition.

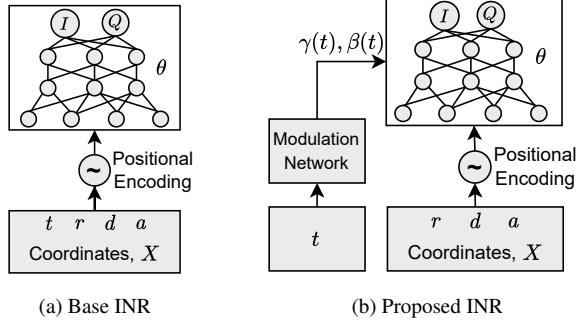


Figure 2. Implicit Neural Networks.

mmWave Signal Generation: RF-Genesis [4] generates high-quality mmWave signals using simulation and ray tracing but requires 20 seconds to 2 minutes per signal, while RF-Diffusion [5] uses time-frequency diffusion but produces lower-quality signals. Neither approach addresses novel signal encoding, efficient representation, or super-resolution, and mmWeaver is the first framework to explore these aspects.

3. Methodology

3.1. Signal Representation

In this section, we present our methodology for extracting task-invariant and compressed signal representations using implicit neural representations (INRs). First, we validate the ability of INRs to model individual instances of complex signals, such as mmWave radar data, with high fidelity. Next, we extend this framework by integrating hypernetworks with the INRs, enabling the development of a generalized representation capable of capturing the entire signal space across diverse environments and activities.

3.1.1. INR for RF representation

Background: Implicit Neural Representations (INRs) are a powerful technique for modeling discretely sampled signals as continuous functions. An INR, f_θ , typically employs fully connected layers to map input coordinates \mathbf{X} to their corresponding signal values, enabling efficient encoding of high resolution data and supporting tasks like interpolation and super-resolution. For temporally varying signals, such as mmWave radar data, the input coordinates are extended to $\mathbf{X} = (t, r, d, a)$, where t represents time, r denotes range, d indicates Doppler frequency, and a specifies the antenna index (azimuth or elevation). This basic formulation allows the INR to capture the spatio-temporal dynamics of mmWave signals, as shown in Figure 2a as *Base INR*, enabling detailed and continuous modeling of such data.

Limitation: The base architecture conflates spatial and temporal domains, making it inefficient for capturing temporal dynamics and requiring a larger number of param-

eters to model mmWave signals effectively. This inefficiency arises because, during human activity sensing, only a small subset of range or Doppler indices change between consecutive frames. As a result, using separate INR weights for each sparse radar frame becomes highly redundant and computationally inefficient.

Proposed Architecture: To address the limitations, we propose an enhanced architecture that decouples temporal patterns from spatial features by introducing a dedicated temporal encoding module. This separation enables the model to better capture human motion dynamics, improving both efficiency and representation performance. In Figure 2b, we present our decoupled architecture that incorporates a temporal modulation network. This network maps temporal inputs t to modulation vectors $\gamma(t), \beta(t)$. The input to the INR is the coordinate tuple $\mathbf{X} = (r, d, a)$, which is fed to the Fourier-based positional encoder [37] layer, PE , which maps X to a higher-dimensional space using exponentially scaled frequencies. This encoding captures both low- and high-frequency variations, enabling the model to represent fine-grained and global details effectively:

$$PE(\mathbf{X}) = [\cos(2^i \mathbf{X}), \sin(2^i \mathbf{X})]_{i=0}^L$$

where L is the number of frequencies used. For our designed INRs, we set $L = 8$, which maps input coordinates $\mathbf{X} \in \mathbb{R}^3$ to a positional encoding $PE(\mathbf{X}) \in \mathbb{R}^{51}$, resulting in a 51-dimensional vector.

The positional encoding vectors are then passed through a series of MLP layers, which share common weights θ across all frames in a sequence. The output of each layer L is modulated by a scale factor $\gamma(t)$ and a shift factor $\beta(t)$, both dependent on time t . The network output is expressed as:

$$f_\theta(\mathbf{X}; t) = \sigma_L(\gamma_L(t) \odot (\mathbf{W}_L \sigma_{L-1}(\dots) + \mathbf{b}_L) + \beta_L(t)),$$

where σ_L is the ReLU [17] activation function at layer L , \mathbf{W}_L and \mathbf{b}_L are the weight matrix and bias vector, and \odot denotes element-wise multiplication.

Sampling: After computing the network output $f_\theta(\mathbf{X}; t)$, we can sample the signal at each discrete value of \mathbf{X} to generate the complete mmWave signal. Sampling at finer intervals within the range of these indices enables higher-resolution data generation. For instance, let the original sampling intervals for range, Doppler, and azimuth be $\Delta r, \Delta d, \Delta a$, respectively. By downscaling these intervals by factors n_r, n_d, n_a , the resolution increases proportionally, and the total number of sampled points becomes:

$$N_{\text{new}} = n_r \cdot n_d \cdot n_a \cdot N_{\text{orig}},$$

where N_{orig} is the number of original discrete sampling points. This capability facilitates the generation of multi-resolution mmWave data. Additionally, sampling within a

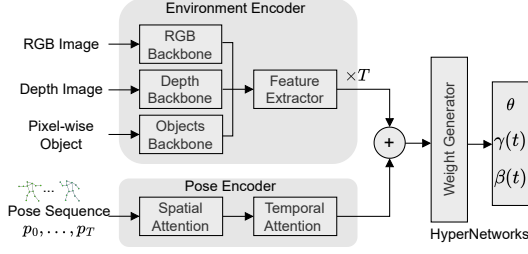


Figure 3. Hypernetwork architecture with environment and pose encoders for generating INR weights.

controlled error range around discrete coordinates allows for augmenting existing datasets, introducing realistic variability without compromising the data’s integrity.

3.1.2. Generalization via Hypernetworks

As shown in Section 3.1.1, INRs can represent discrete RF signals as continuous functions, enabling compression and super-resolution. However, training a separate INR for each signal instance is computationally expensive. The key challenge is to generalize signal representation across diverse environments and motions by mapping environmental and motion features to corresponding RF signals.

To this end, we leverage hypernetworks—meta-models that generate weights for target networks. Since RF propagation depends on both static environmental structures (e.g., walls, furniture) and dynamic human motion, we use two specialized encoders to extract relevant features. The hypernetwork uses these to generate INR weights θ , and modulation vectors $\gamma(t)$, $\beta(t)$, enabling signal generalization across scenes and activities with high fidelity.

Environment Encoder: The encoder processes RGB images, depth maps, and object detection masks [13] pre-trained on COCO-Stuff [2]. A CNN based on EfficientNet-B0 [25] extracts 512-dimensional spatial features $\mathbf{z}_e \in \mathbb{R}^{512}$, balancing accuracy and efficiency across multimodal inputs.

Pose Encoder: Given 3D pose sequences $\{\mathbf{p}_t \in \mathbb{R}^{J \times 3}\}_{t=1}^T$, a two-stage Transformer encoder captures spatial and temporal dependencies. Each pose \mathbf{p}_t is embedded via a fully connected layer: $\mathbf{h}_t = \text{FC}(\mathbf{p}_t) \in \mathbb{R}^d$, then processed via spatial and temporal self-attention to yield a latent sequence $\mathbf{z}_p \in \mathbb{R}^{T \times 512}$.

Hypernetwork: The environmental encoding \mathbf{z}_e is broadcasted over time and concatenated with \mathbf{z}_p . This joint representation is passed through MLP layers to generate the INR weights θ and modulation vectors $\gamma(t)$, $\beta(t)$, which condition the INR to synthesize the radar signal at all spatial coordinates.

3.2. Signal Generation

After training the INR and hypernetwork to map motion sequences to mmWave signals, we generate diverse synthetic data using MotionGPT [11], a Transformer-based model for human motion synthesis. Given a motion prompt, MotionGPT produces temporally coherent 3D pose sequences by modeling spatial-temporal dependencies with multi-head self-attention. For each scene, the environment encoder extracts a feature vector \mathbf{z}_e from an RGB-D image, while MotionGPT-generated poses are encoded into latent motion vectors $\mathbf{Z}_p = \{\mathbf{z}_p(t)\}_{t=1}^T$. These are fused in the hypernetwork to generate INR parameters, which are sampled over (r, d, a, t) to synthesize complex-valued mmWave signals. Repeating this process across varied prompts and environments yields diverse, realistic signals that augment training data.

4. Experimental Setup

4.1. Dataset Collection

We construct a diverse dataset to develop and evaluate our mmWave generation framework. mmWave data is captured using a TI AWR1843 radar [26] (77–81 GHz, 3 TX/4 RX, 4.4 cm range resolution), and visual data with an Intel RealSense D455 depth camera [10] (1280 × 720). Both devices, housed in a custom case and connected to a Linux machine, are synchronized via timestamps (Figure 4b); the radar streams at 10 fps and the camera at 15 fps.

We collect data in 10 indoor scenes (offices, living rooms, labs, kitchens, libraries) with varied layouts and materials (Figure 4a). To increase diversity, we rearrange furniture, vary participant positions/orientations 5–10× per scene, and record six participants (ages 25–60, heights 5’4”–6’5”) performing 12 predefined activities (*waving, clapping, jogging, jumping jacks, walking, etc.*), repeated multiple times. This yields over 12,000 frame sequences, providing a diverse dataset collected under our institution’s IRB protocol.

4.2. Model Training

The *Signal Representation Module* learns a continuous function to model mmWave signals based on environmental features and human motion. It is trained using a combination of Complex SSIM Loss, Mean Squared Error (MSE) Loss, and Perceptual Loss. Perceptual Loss is an L_1 loss applied to features extracted via a custom convolution-based mmWave feature extractor to capture high-level signal characteristics. Training runs for 1,000 epochs using the Adam optimizer with a learning rate of 1×10^{-4} . At each epoch, the INR is sampled at 16,384 points from 131,072 spatial-temporal coordinates (r, d, a, t) , prioritizing range indices with detected human activity while ensuring domain cover-



(a) Synchronized mmWave and video data are recorded in diverse environments; four examples are shown.

(b) Device Setup.

Figure 4. Examples of indoor environments and the device setup.

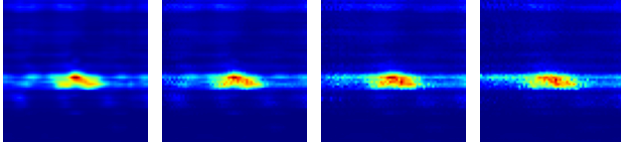


Figure 5. Range-azimuth spectrograms of generated signals at four sampling radii: 0, 1, 2, and 3 (from left to right).

age through random sampling. The total loss function is:

$$\mathcal{L}_{\text{INR}} = \lambda_{\text{SSIM}} \mathcal{L}_{\text{SSIM}} + \lambda_{\text{MSE}} \mathcal{L}_{\text{MSE}} + \lambda_{\text{Perceptual}} \mathcal{L}_{\text{Perceptual}},$$

where λ_{SSIM} , λ_{MSE} , $\lambda_{\text{Perceptual}}$ weight each term. We tuned $\lambda_{\text{SSIM}}=0.5$, $\lambda_{\text{MSE}}=0.3$, $\lambda_{\text{Perceptual}}=0.2$ on a validation split to balance fidelity and downstream utility. For a single signal instance, an INR is trained for 500 epochs with a learning rate of 1×10^{-4} .

4.3. Microbenchmarks

mmWeaver consists of an *Environment Encoder* (2.1M parameters) for extracting spatial features from RGB-D images, a *Pose Encoder* (4.9M) for capturing human motion, and a hypernetwork with supporting modules, totaling 14.73M trainable parameters. Each 20-frame sequence is represented by an INR with 10,018 parameters—4,898 for shared weights (θ) and 5,120 for time-dependent modulations ($\gamma(t)$, $\beta(t)$) across frames. Training and inference run on an NVIDIA RTX 4090 GPU (24 GB), where generating a 20-frame sequence takes 3.4s, compared to 20s–2 min for RF-Genesis [4], highlighting mmWeaver’s efficiency in high-resolution signal synthesis.

4.4. Evaluation Metrics

We evaluate mmWeaver using a comprehensive set of metrics across signal quality, representation accuracy, and downstream performance.

SSIM [29] and cSSIM: SSIM compares structural features such as luminance and contrast. For complex-valued mmWave signals, we use cSSIM, which separately evaluates the real and imaginary components to preserve both magnitude and phase information.

PSNR [7]: PSNR measures reconstruction fidelity based on the ratio between the maximum signal value and the

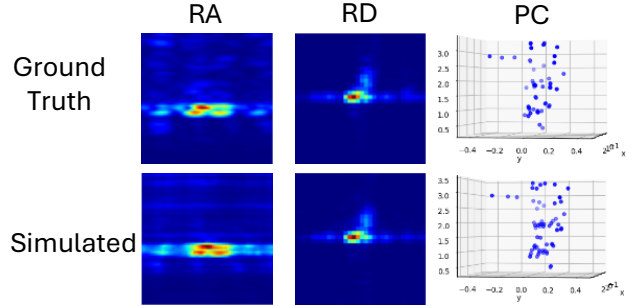


Figure 6. mmWeaver-generated signal in range-azimuth, range-doppler spectrogram, and point cloud format.

mean squared error, with higher values indicating better signal quality.

INR Evaluation: To assess the INR’s super-resolution and representation capabilities, we use cSSIM, MSE, and activity recognition accuracy. The latter is computed using a 12-class classifier trained on mmWave signals at different resolutions.

Point Cloud Evaluation: We use Hausdorff distance [9] to measure geometric similarity between predicted and ground-truth point clouds, capturing maximum spatial deviation in 3D.

Downstream Task Evaluation: To demonstrate real world utility, we fine-tune pretrained pose and action recognition models on mmWeaver-generated signals in unseen environments, evaluating improvements in accuracy and robustness.

4.5. Baselines

To evaluate the effectiveness of data generation and augmentation, we utilize two baseline approaches for downstream tasks: mmMesh [31] for human pose estimation and the DRAI-based approach [15] for human activity recognition. Additionally, we enhance the performance of these baseline models through environment-specific data augmentation provided by mmWeaver, as well as two alternative data generation methods: RF-Genesis [4], which employs physical simulation for synthetic RF data, and the time-frequency diffusion-based approach RF-Diffusion [5].

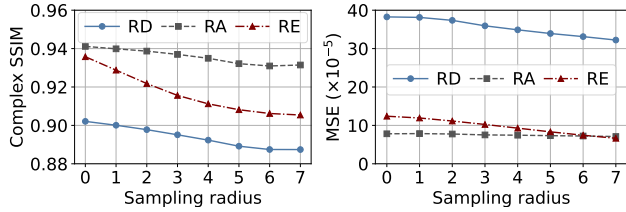


Figure 7. Data augmentation using different sampling.

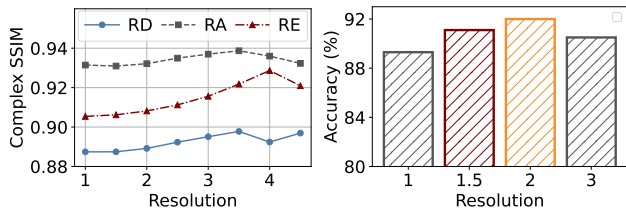


Figure 8. Benefits of higher resolution sampling using INR.

5. Evaluation

5.1. Evaluation of INR

Using Implicit Neural Representations (INRs) to model continuous complex signals such as mmWave radar provides significant advantages beyond synthetic signal generation. In this section, we discuss the benefits of using INRs to augment and enhance existing mmWave radar data for downstream tasks.

Data Augmentation: INRs provide a key advantage by learning a continuous function f_θ over discretely sampled signals, enabling sampling at arbitrary coordinates. For example, given a radar signal with 64 discrete range indices, an INR trained on these indices can generate values at intermediate points (e.g., range index 1.1), facilitating systematic data augmentation. This approach introduces realistic, controllable variations into the dataset, enhancing its diversity and robustness.

To evaluate augmentation, we divide index intervals into 8 parts and define a *sampling radius* $r \in [0, 7]$. At coordinate j , samples are drawn from $[j, j + \frac{r}{8}]$ and quality is measured via cSSIM and MSE on range-Doppler (RD), range-Azimuth (RA), and range-Elevation (RE) spectrograms (Figure 7). For $r \leq 2$, scores remain close to the original ($r = 0$), with cSSIM dropping only 0.05–0.12 for RD/RA, while RE shows larger drops due to limited elevation resolution. Visualizations in Figure 5 confirm high-fidelity RA spectrograms at $r = 1, 2, 3$. These results demonstrate that INRs can augment mmWave datasets by varying spatial sampling, improving robustness of downstream models to signal variation and noise.

Super Resolution: Another significant advantage of learning a continuous function over discretely sampled signals is the ability to perform super-resolution by sampling at aug-

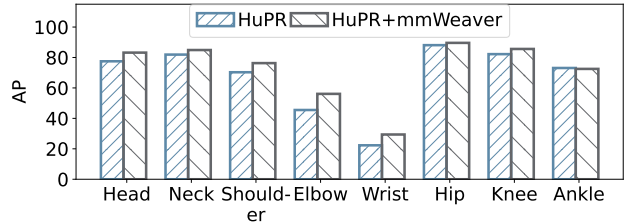


Figure 9. Joint-wise comparison on HuPR dataset.

mented intermediate coordinates. For example, instead of sampling at discrete range indices $[0, 1, \dots, 64]$, we can sample at finer intervals, such as $[0, 0.5, 1, \dots, 64]$, effectively doubling the resolution of the original signal. This enables the generation of higher-resolution signals while preserving the underlying structure of the data. If the INR is well-fitted to the original signal, higher-resolution sampling enhances fine-grained information, which is expected to increase SSIM scores and improve downstream task performance.

We evaluate the impact of super-resolution in Figure 8, where SSIM scores are reported for range-Doppler (RD), range-Azimuth (RA), and range-Elevation (RE) spectrograms at resolutions upto $4\times$ the original coordinates. The results demonstrate consistent improvements in SSIM scores across all spectrogram types with increasing resolution, indicating the fidelity of the super-resolved signals. Furthermore, we assess downstream task performance by training a baseline human activity recognition model on the original signal and high-resolution signals sampled at $1.5\times$, $2\times$ and $3\times$ resolutions. The higher resolution signals yield 1–3% improved recognition accuracy, showcasing the efficacy of super-resolution in enhancing both signal quality and downstream task outcomes.

Compression: Our network uses 10,018 parameters to model data of size $10 \times 64 \times 32 \times 12 \times 2 = 491,520$ points, yielding a compression ratio of $\frac{491,520}{10,018} \approx 49.06$.

5.2. Evaluation of Signal Generation

We evaluate mmWeaver against RF-Genesis and RF-Diffusion using SSIM, PSNR, and Hausdorff Distance. SSIM and PSNR measure perceptual similarity and signal fidelity, respectively, while Hausdorff Distance quantifies geometric alignment between predicted and ground-truth point clouds. Higher SSIM/PSNR and lower Hausdorff values indicate better signal quality. Since text-conditioned generation yields multiple plausible outputs, we use controlled settings where synthetic signals are generated from exact 3D pose sequences for fair comparison.

As shown in Figure 10, mmWeaver achieves the highest SSIM (0.88) and PSNR (35 dB), outperforming RF-Genesis (0.86, 33.2 dB) and RF-Diffusion (0.75, 31.6 dB). For point cloud evaluation, mmWeaver achieves the lowest Hausdorff Distance (0.32 m) versus RF-Genesis (0.37 m). Figure 6

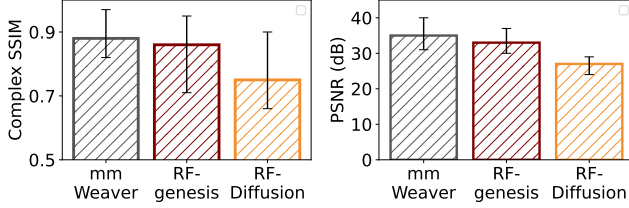


Figure 10. Comparison of quality of generated signal.

shows sample RA/RD spectrograms and point clouds, illustrating mmWeaver’s fidelity and structural accuracy. These results confirm mmWeaver’s ability to synthesize perceptually and geometrically realistic mmWave signals.

5.3. Generalization Across Unseen Environments

We evaluate the robustness of mmWeaver by categorizing three unseen test environments into clutter levels—*low*, *medium*, and *high*—based on furniture density and occluders: a lab with minimal objects, a living room with standard furniture, and a small kitchen with dense clutter. Using the same set of activities, we augment training data with mmWeaver-generated signals conditioned on the corresponding RGB-D priors and evaluate on unseen HAR tasks. In low clutter, we obtain cSSIM of 0.89 and HAR accuracy of 90.6%; in medium clutter, cSSIM 0.87 and HAR 91.0%; and in high clutter, cSSIM 0.84 and HAR 86.7%. These results show that mmWeaver preserves fidelity and recognition accuracy in simple and moderately complex scenes, with only modest degradation in highly cluttered scenes. Importantly, even in the most challenging case, mmWeaver improves HAR performance (86.7%) over the baseline (83.2%), demonstrating robustness and consistent benefit.

5.4. Generalization Across Unseen Activities

We assess activity generalization by withholding two actions during training. For *right-hand raise*, structurally similar to the trained *left-hand raise*, mmWeaver generated signals achieve 87.4% accuracy, showing extrapolation to related motions. For the novel action *jumping*, accuracy drops to 78.1%, reflecting the challenge of unseen activities. However, due to the modular design with separate encoders for activities and environments, mmWeaver adapts quickly: fine-tuning on a small set of *jumping* samples in one environment raises accuracy to 85.6% across all environments. Thus, while zero-shot generalization to arbitrary activities is challenging, efficient adaptation is possible with minimal data.

5.5. Evaluation on Public Dataset

To assess mmWeaver’s generalizability, we conduct experiments on the public HuPR [14] dataset and model for

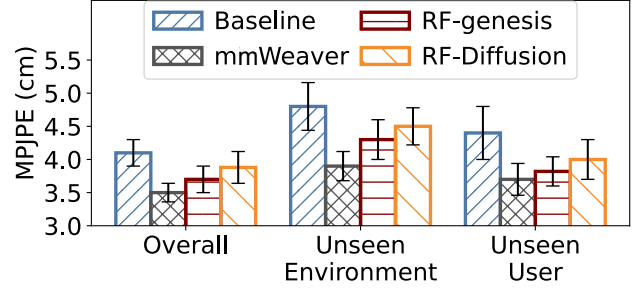


Figure 11. Comparison of human pose estimation error.

mmWave-based human pose estimation. HuPR contains 235 video sequences (60s each at 10 FPS), split into 193 training, 21 validation, and 21 test samples. As HuPR lacks explicit RGB-D scans of empty environments, we use the first video frame as a proxy. HuPR also uses two mmWave radars (horizontal and vertical), requiring two INRs per sequence to model dual perspectives.

To augment training, we map pose sequences from the evaluation set to mmWave signals via 1-to-1 mappings and apply structured random sampling for additional diversity. This increases variation in motion and context, improving generalization. We compare the baseline HuPR model trained on original data with HuPR+mmWeaver, trained using both original and mmWeaver-augmented data.

Figure 9 shows Average Precision (AP) across joints for both models. HuPR+mmWeaver outperforms the baseline across all joints, with the largest gains in distal joints (elbow, wrist, knee) that are typically harder to localize due to occlusion and fast motion. These results validate the effectiveness of mmWeaver-based signal generation for public dataset enhancement.

6. Case Studies

6.1. Human Pose Estimation

Human pose estimation is vital for applications like indoor monitoring and surveillance. In this section, we evaluate mmWeaver’s effectiveness in enhancing pose estimation by augmenting existing mmWave datasets with high-quality, environment-specific synthetic data.

6.1.1. Experiment Design:

We use pose data from 12 activities (Section 4.1) and generate 1,000 synthetic samples per method—RF-Genesis, RF-Diffusion, and mmWeaver—to fine-tune a baseline pose estimation model. For mmWeaver, samples are generated across all activities and environments for overall comparison. We further evaluate generalization in two scenarios: unseen users and unseen environments. In the latter, mmWeaver generates synthetic data conditioned solely on RGB-D images and textual descriptions, requiring no real signal collection during testing. Additionally, we ap-

ply our INR-based data augmentation strategy during fine-tuning. This setup enables a comprehensive evaluation of mmWeaver’s effectiveness across varied pose estimation scenarios.

6.1.2. Overall Evaluation:

For the overall evaluation, we allocate 80% of the total data for training and reserve the remaining 20% for testing. As shown in Figure 11, the baseline model achieves an average pose estimation error of 4.1 cm in terms of MPJPE. When the dataset is augmented with synthetic data generated by mmWeaver, RF-Genesis, and RF-Diffusion, followed by fine-tuning, the MPJPE decreases to 3.5 cm, 3.72 cm, and 3.85 cm, respectively. These results highlight the effectiveness of dataset augmentation using synthetic data, particularly with mmWeaver, which outperforms other methods. Additionally, the results emphasize the importance of combining new synthetic datasets with existing data augmentation techniques to improve pose estimation accuracy.

6.1.3. Unseen Environment Evaluation:

To evaluate performance in unseen environments, we reserve 2 of the 10 environments for testing and generate synthetic data using mmWeaver. Results are compared against RF-Genesis and RF-Diffusion, which do not account for environment. As shown in Figure 11, incorporating environment-specific synthetic data reduces MPJPE by 1.0 cm, surpassing the 0.6 cm and 0.4 cm gains of RF-Genesis and RF-Diffusion. We further ablate environment priors by replacing exact priors with generic ones, yielding a 0.7 cm MPJPE reduction—comparable to environment-generic baselines but below the 1.0 cm achieved with mmWeaver using exact priors.

6.1.4. Unseen User Evaluation:

Using a leave-one-out strategy across six users, mmWeaver achieves 3.7 cm MPJPE compared to 4.4 cm baseline, outperforming RF-Genesis (3.8 cm) and RF-Diffusion (3.9 cm). While average MPJPE gains may appear modest, improvements of 0.6–1.1 cm span 17 joints. Notably, some critical joints exhibit reductions up to 10.45 cm, significantly enhancing downstream gesture and pose-based tasks.

6.2. Human Activity Recognition

Human activity recognition is critical for downstream tasks in applications such as indoor monitoring and behavioral analysis. In this section, we evaluate the capability of mmWeaver to improve the performance of a baseline activity recognition model through synthetic data generation and augmentation.

6.2.1. Experiment Design:

Similar to previous case study for human pose estimation, we evaluate activity recognition performance across

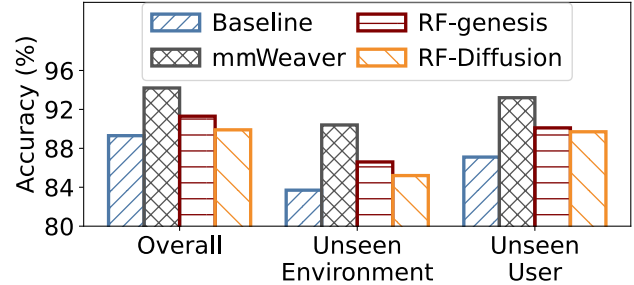


Figure 12. Comparison of human activity recognition.

three scenarios: overall performance, unseen environments, and unseen users. Synthetic datasets are generated using mmWeaver, RF-Genesis, and RF-Diffusion, and the baseline model is fine-tuned with these augmented datasets. Classification accuracy is used as the evaluation metric, and results are reported in Figure 12.

6.2.2. Results:

The baseline model achieves 89.3% accuracy, which rises to 94.2% with mmWeaver-generated data. RF-Genesis and RF-Diffusion yield 91.3% and 89.9%, respectively. For unseen environments, mmWeaver reaches 90.4%, outperforming RF-Genesis (86.6%), RF-Diffusion (85.2%), and the baseline (83.7%). We also ablate environment priors by replacing exact priors with generic ones, yielding 87.2% accuracy—above the 83.7% baseline but below the 90.4% achieved with exact priors. For unseen users, mmWeaver attains 93.2% accuracy, outperforming RF-Genesis (90.1%) and RF-Diffusion (89.7%), as well as the baseline (87.1%).

7. Conclusion

We presented mmWeaver, a framework that models mmWave signals as continuous functions using Implicit Neural Representations (INRs), achieving 49× compression and enabling multi-resolution sampling for data augmentation. To generalize across environments and activities, mmWeaver employs hypernetworks conditioned on environmental and motion features, while a generative model synthesizes diverse motions to produce realistic, scenario-specific signals. Extensive evaluations show that mmWeaver outperforms prior methods, improving both pose estimation and activity recognition. However, our system is currently evaluated on single-person scenarios; extending to multi-person cases is feasible (e.g., by superimposing signals of separated users), though handling close interactions remains an open challenge. Our setup also assumes a TI AWR1843 radar; while higher resolution can be approximated via augmented sampling, substantially higher-resolution radars would require hypernetwork fine-tuning. Future work will focus on optimizing INR efficiency, incorporating additional modalities and hardware, and broadening task applicability.

Acknowledgments

This work was supported in part by the National Science Foundation under NSF Awards 2503073 and 2047461.

References

- [1] Sizhe An, Yin Li, and Umit Ogras. mri: Multi-modal 3d human pose estimation dataset using mmwave, rgb-d, and inertial sensors. *Advances in Neural Information Processing Systems*, 35:27414–27426, 2022. 1, 2
- [2] Holger Caesar, Jasper Uijlings, and Vittorio Ferrari. Cocomstuff: Thing and stuff classes in context. In *Proceedings of the IEEE conference on computer vision and pattern recognition*, pages 1209–1218, 2018. 4
- [3] Qiming Cao, Hongfei Xue, Tianci Liu, Xingchen Wang, Haoyu Wang, Xincheng Zhang, and Lu Su. mmclip: Boosting mmwave-based zero-shot har via signal-text alignment. In *Proceedings of the 22nd ACM Conference on Embedded Networked Sensor Systems*, pages 184–197, 2024. 2
- [4] Xingyu Chen and Xinyu Zhang. Rf genesis: Zero-shot generalization of mmwave sensing through simulation-based data synthesis and generative diffusion models. In *Proceedings of the 21st ACM Conference on Embedded Networked Sensor Systems*, page 28–42, New York, NY, USA, 2024. Association for Computing Machinery. 2, 3, 5
- [5] Guoxuan Chi, Zheng Yang, Chenshu Wu, Jingao Xu, Yuchong Gao, Yunhao Liu, and Tony Xiao Han. Rf-diffusion: Radio signal generation via time-frequency diffusion. In *Proceedings of the 30th Annual International Conference on Mobile Computing and Networking*, pages 77–92, 2024. 2, 3, 5
- [6] David Ha, Andrew Dai, and Quoc V Le. Hypernetworks. *arXiv preprint arXiv:1609.09106*, 2016. 2
- [7] Alain Horé and Djemel Ziou. Image quality metrics: Psnr vs. ssim. In *2010 20th International Conference on Pattern Recognition*, pages 2366–2369, 2010. 5
- [8] Hao Huang, Guan Gui, H. Gađanin, C. Yuen, H. Sari, and F. Adachi. Deep regularized waveform learning for beam prediction with limited samples in non-cooperative mmwave systems. *IEEE Transactions on Vehicular Technology*, 2023. 2
- [9] D.P. Huttenlocher, G.A. Klanderman, and W.J. Rucklidge. Comparing images using the hausdorff distance. *IEEE Transactions on Pattern Analysis and Machine Intelligence*, 15(9):850–863, 1993. 5
- [10] Intel Corporation. Intel realsense depth camera d455, 2023. Accessed: 2023-12-05. 4
- [11] Biao Jiang, Xin Chen, Wen Liu, Jingyi Yu, Gang Yu, and Tao Chen. Motiongpt: Human motion as a foreign language, 2023. 4
- [12] Feng Jin, Renyuan Zhang, Arindam Sengupta, Siyang Cao, Salim Hariri, Nimit K Agarwal, and Sumit K Agarwal. Multiple patients behavior detection in real-time using mmwave radar and deep cnns. In *2019 IEEE Radar Conference (RadarConf)*, pages 1–6. IEEE, 2019. 1
- [13] Alexander Kirillov, Eric Mintun, Nikhila Ravi, Hanzi Mao, Chloe Rolland, Laura Gustafson, Tete Xiao, Spencer Whitehead, Alexander C Berg, Wan-Yen Lo, et al. Segment anything. In *Proceedings of the IEEE/CVF International Conference on Computer Vision*, pages 4015–4026, 2023. 4
- [14] Shih-Po Lee, Niraj Prakash Kini, Wen-Hsiao Peng, Ching-Wen Ma, and Jenq-Neng Hwang. Hupr: A benchmark for human pose estimation using millimeter wave radar. In *Proceedings of the IEEE/CVF Winter Conference on Applications of Computer Vision*, pages 5715–5724, 2023. 1, 2, 7
- [15] Yadong Li, Dongheng Zhang, Jinbo Chen, Jinwei Wan, Dong Zhang, Yang Hu, Qibin Sun, and Yan Chen. Towards domain-independent and real-time gesture recognition using mmwave signal. *IEEE Transactions on Mobile Computing*, 22(12):7355–7369, 2022. 2, 5
- [16] Mahathir Monjur and Shahriar Nirjon. Voicedirect: mmwave and audio signal fusion for user localization and speaking direction estimation. In *The 21st International Conference on Embedded Wireless Systems and Networks(EWSN)*, 2024. 1, 2
- [17] Johannes Schmidt-Hieber. Nonparametric regression using deep neural networks with relu activation function. 2020. 3
- [18] Arindam Sengupta, Feng Jin, Renyuan Zhang, and Siyang Cao. mm-pose: Real-time human skeletal posture estimation using mmwave radars and cnns. *IEEE Sensors Journal*, 20(17):10032–10044, 2020. 1, 2
- [19] Akash Deep Singh, Sandeep Singh Sandha, Luis Garcia, and Mani Srivastava. Radhar: Human activity recognition from point clouds generated through a millimeter-wave radar. In *Proceedings of the 3rd ACM Workshop on Millimeter-wave Networks and Sensing Systems*, pages 51–56, 2019. 1, 2
- [20] Vincent Sitzmann, Julien Martel, Alexander Bergman, David Lindell, and Gordon Wetzstein. Implicit neural representations with periodic activation functions. *Advances in neural information processing systems*, 33:7462–7473, 2020. 2
- [21] Ivan Skorokhodov, Savva Ignatyev, and Mohamed Elhoseiny. Adversarial generation of continuous images. In *Proceedings of the IEEE/CVF conference on computer vision and pattern recognition*, pages 10753–10764, 2021. 2
- [22] Yannick Strümler, Janis Postels, Ren Yang, Luc Van Gool, and Federico Tombari. Implicit neural representations for image compression. In *European Conference on Computer Vision*, pages 74–91. Springer, 2022. 2
- [23] Kun Su, Mingfei Chen, and Eli Shlizerman. Inras: Implicit neural representation for audio scenes. *Advances in Neural Information Processing Systems*, 35:8144–8158, 2022. 2
- [24] Filip Szatkowski, Karol J Piczak, Przemysław Spurek, Jacek Tabor, and Tomasz Trzcieski. Hypersound: Generating implicit neural representations of audio signals with hypernetworks. *arXiv preprint arXiv:2211.01839*, 2022. 2
- [25] Mingxing Tan. Efficientnet: Rethinking model scaling for convolutional neural networks. *arXiv preprint arXiv:1905.11946*, 2019. 4
- [26] Texas Instruments. Awr1843: 77-ghz radar-on-chip device, 2023. Accessed: 2023-12-05. 4
- [27] Shelly Vishwakarma, Wenda Li, Chong Tang, Karl Woodbridge, Raviraj Adiv, and Kevin Chetty. Simhualator: An open-source end-to-end radar simulator for human activity recognition. *IEEE Aerospace and Electronic Systems Magazine*, 37(3):6–22, 2021. 2

- [28] Yuheng Wang, Haipeng Liu, Kening Cui, Anfu Zhou, Wensheng Li, and Huadong Ma. m-activity: Accurate and real-time human activity recognition via millimeter wave radar. In *ICASSP 2021-2021 IEEE International Conference on Acoustics, Speech and Signal Processing (ICASSP)*, pages 8298–8302. IEEE, 2021. [1](#), [2](#)
- [29] Zhou Wang, A.C. Bovik, H.R. Sheikh, and E.P. Simoncelli. Image quality assessment: from error visibility to structural similarity. *IEEE Transactions on Image Processing*, 13(4): 600–612, 2004. [5](#)
- [30] Zhiming Wang, Dechen Jiang, Bin Sun, and Y. Wang. A data augmentation method for human activity recognition based on mmwave radar point cloud. *IEEE Sensors Letters*, 2023. [2](#)
- [31] Hongfei Xue, Yan Ju, Chenglin Miao, Yijiang Wang, Shiyang Wang, Aidong Zhang, and Lu Su. mmmesh: towards 3d real-time dynamic human mesh construction using millimeter-wave. In *Proceedings of the 19th Annual International Conference on Mobile Systems, Applications, and Services*, page 269–282, New York, NY, USA, 2021. Association for Computing Machinery. [2](#), [5](#)
- [32] Hongfei Xue, Qiming Cao, Chenglin Miao, Yan Ju, Haochen Hu, Aidong Zhang, and Lu Su. Towards generalized mmwave-based human pose estimation through signal augmentation. In *Proceedings of the ACM Conference*. ACM, 2023. [2](#)
- [33] Yiying Yang, Fukun Yin, Wen Liu, Jiayuan Fan, Xin Chen, Gang Yu, and Tao Chen. Pm-inr: Prior-rich multi-modal implicit large-scale scene neural representation. In *Proceedings of the AAAI Conference on Artificial Intelligence*, pages 6594–6602, 2024. [2](#)
- [34] Zhicheng Yang, Parth H Pathak, Yunze Zeng, Xixi Liran, and Prasant Mohapatra. Monitoring vital signs using millimeter wave. In *Proceedings of the 17th ACM international symposium on mobile ad hoc networking and computing*, pages 211–220, 2016. [1](#)
- [35] Zhicheng Yang, Parth H Pathak, Yunze Zeng, Xixi Liran, and Prasant Mohapatra. Vital sign and sleep monitoring using millimeter wave. *ACM Transactions on Sensor Networks (TOSN)*, 13(2):1–32, 2017. [1](#)
- [36] Xiaotong Zhang, Zhenjiang Li, and Jin Zhang. Synthesized millimeter-waves for human motion sensing. In *Proceedings of the 20th ACM Conference on Embedded Networked Sensor Systems*, pages 377–390, 2022. [2](#)
- [37] Jianqiao Zheng, Sameera Ramasinghe, and Simon Lucey. Rethinking positional encoding. *arXiv preprint arXiv:2107.02561*, 2021. [3](#)